JOURNAL OF GEOPHYSICAL RESEARCH, VOL. 87, NO. A7, PAGES 5081–5094, JULY 1, 1982

The Structure of Perpendicular Bow Shocks

M. M. LEROY,[1] D. WINSKE, C. C. GOODRICH, C. S. WU, AND K. PAPADOPOULOS

University of Maryland, College Park, Maryland 20742

A hybrid simulation model with kinetic ions, massless fluid electrons, and phenomenological resistivity is used to study the perpendicular configuration of the bow shocks of the earth and other planets. We investigate a wide range of parameters, including the upstream Mach number, electron and ion beta (ratios of thermal to magnetic pressure), and resistivity. Electron beta and resistivity are found to have little effect on the overall shock structure. Quasi-stationary structures are obtained at moderately high ion beta ($\beta_i \sim 1$), whereas the shock becomes more dynamic in the low ion beta, large Mach number regime ($\beta_i \sim 0.1$, $M_A > 8$). The simulation results are shown to be in good agreement with a number of observational features of quasi-perpendicular bow shocks, including the morphology of the reflected ion stream, the magnetic field profile throughout the shock, and the Mach number dependence of the magnetic field overshoot.

1. INTRODUCTION

Satellite observations of the earth's bow shock provide a powerful tool for investigating collisionless shock waves in the high Mach number regime. Reviews of the earlier observations may be found in the articles by *Formisano* [1977] and *Greenstadt and Fredricks* [1979]. The recent ISEE data have shed new light on the subject, not only because of better time resolution but also because the use of two spacecraft has permitted a reliable determination of the shock thickness. One of the numerous results of the ISEE mission has been a description of the overall structure of a typical transition layer in a quasi-perpendicular high Mach number bow shock. The magnetic field structure, analyzed by the high resolution magnetometer experiment [*Russell and Greenstadt*, 1979], usually consists of a foot region which scales as c/ω_{pi} (ω_{pi} is the upstream ion plasma frequency), a thin ($\ll c/\omega_{pi}$) magnetic ramp or shock front, followed by a postgradient overshoot scaling as several c/ω_{pi}.

Preliminary analysis of ion distribution functions from the LASL/MPE fast plasma experiment [*Bame et al.*, 1979] indicates that a population of about 20% of the incoming ions is reflected in the foot region [*Paschmann et al.*, 1981]. These ions eventually reach the downstream region apparently without thermalizing rapidly, confirming the earlier observations by *Montgomery et al.* [1970].

The ion reflection phenomenon associated with high Mach number perpendicular shocks, i.e., Alfvén Mach number larger than about 3, has been theoretically investigated mainly by means of numerical simulation. Thus *Papadopoulos et al.* [1971], *Forslund and Freidberg* [1971], and *Mason* [1972] have analyzed situations in which the ions are unmagnetized with particle in cell codes. The case of magnetized ions has been treated by *Auer et al.* [1962] and *Auer and Evers* [1971], using charge sheets, and by *Biskamp and Welter* [1972] with a particle code. Such simulations have greatly advanced our knowledge of collisionless shock waves. In particular, *Auer et al.* [1962, 1971] have identified the bimodal ion distributions observed in the downstream region of the bow shock by *Montgomery et al.* [1970] as an ion stream gyrating in the downstream magnetic field, while *Forslund and Freidberg* [1971] have clarified the role and properties of the critical Mach numbers associated with ion reflection.

Anomalous resistivity, however, is absent in such simulations because most of the plasma instabilities leading to anomalous resistivity are due to cross field currents and are thus eliminated by the one-dimensionality of these models. *Chodura* [1975] has considered a different model, although still one-dimensional, in which the ions are treated kinetically, the electrons are treated as a fluid, and anomalous resistivity is included in a macroscopic fashion. This model, applied to the case of unmagnetized ions relevant to the Garching theta pinch experiment, has led to remarkably small fractions of ions that are reflected by the shock, less than 20% for $M_A \leq 10$. This number is in agreement with laboratory experiments [*Chodura*, 1975] but is contrary to the cold ion, dissipationless model of *Forslund and Freidberg* [1971], which exhibits total reflection of the incoming ions for Mach numbers $M_A \geq 3.18$ (so-called upper critical Mach number). *Chodura* [1975] has interpreted this discrepancy as due to the possibility in his model of dissipating the energy of the incoming plasma into the electrons via Ohmic heating. Hybrid codes have been shown to be successful in describing other laboratory experiments [*Sgro and Nielson*, 1976; *Hamasaki et al.*, 1977].

In a recent paper, *Leroy et al.* [1981] (hereafter referred to as paper 1) have adopted such a hybrid model for the perpendicular bow shock. The ions are magnetized, and moreover, the shock is not initialized by a driving piston, as in previous simulations, but through the interaction of two plasma streams. The preliminary results presented in paper 1 for a high M_A perpendicular shock indicate that a number of observational features can be understood as consequences of the reflected ions. The overall shock structure consists of several distinct regions whose properties are closely connected to the dynamics of the reflected ions. The shock structure is quasi-stationary and sustained by the ion reflection process. Finally, the reflected ions are magnetically deflected downstream with a kinetic energy per ion significantly larger than the upstream ion kinetic energy.

In this paper we provide a comprehensive analysis of the shock model presented in paper 1 and investigate the behav-

[1] Now at DESPA, Observatoire de Meudon, 92190 Meudon, France.

Paper number 2A0651.
0148-0227/82/002A-0651$05.00

ior of this model over wide ranges of its parameters. We note that large sets of observational data of the earth's and planetary bow shocks, involving different upstream conditions, have been collected during the past decade [*Greenstadt and Fredricks*, 1979; *Russell and Greenstadt*, 1979; *Russell et al.*, 1981]. Thus our investigation not only allows us to determine the parameter range of validity of the results of paper 1, but offers us the opportunity to compare our results with the available observations of quasi-perpendicular bow shocks.

The plan of the paper is as follows. The physical model is presented in section 2. A typical case ($M_A = 6$, $\beta_{e1} = \beta_{i1} = 1$, where β_{e1} and β_{i1} are the upstream ratio of thermal to magnetic pressure for electrons and ions, respectively) is analyzed in section 3. Detailed diagnoses of the time behavior of the shock structure in the simulation are given which confirm the quasi-stationarity of the shock. The role of resistivity and upstream parameters M_A, β_{e1}, β_{i1} is discussed in section 4. It is found that the shock structure does not depend sensitively upon β_{e1} and resistivity, but that the shock behavior is found to be more dynamic (less stationary) at low β_{i1} ($\beta_{i1} \sim 0.1$) than at moderately high β_{i1} ($\beta_{i1} \sim 1$). However, even our low β_{i1} results do not support the results of *Biskamp and Welter* [1972], who have found a periodically vanishing shock front. More significant are the variations of the model with M_A. In the subcritical limit, i.e., M_A smaller than the lower critical Mach number $M_A^* \sim 2.5$, no ion reflection occurs in the model in accordance to fluid theory. For M_A larger than M_A^*, ion reflection occurs simultaneously with the appearance of a magnetic field overshoot. The flux of reflected ions reaches 30–40% of the incoming flux for $M_A \simeq 12$–13. Because the simulation leads to nonstationary structures beyond this value, it is tempting to consider this as the analog in the 'resistive' case of the upper critical Mach number found in the dissipationless model of *Forslund and Freidberg* [1971]. The magnetic field features are found to scale with V_1/ω_{ci2}, where V_1 is the upstream velocity and ω_{ci2} is the gyrofrequency computed with the downstream magnetic field. This scaling is consistent with the discussion of *Morse* [1976]. Section 5 summarizes our results and discusses them in relation to the observations. This discussion is mainly concerned with broad features of observed quasi-perpendicular bow shocks taken as a whole. It will be complemented in a forthcoming paper by a very detailed comparison of our model with one specific shock observation, corresponding to the ISEE shock crossing of November 7, 1977, with a particular emphasis on the comparison of ion distribution functions throughout the shock (C. C. Goodrich, manuscript in preparation, 1982).

2. Physical Model

The numerical simulations have been performed with the hybrid code used in paper 1, in which the ions are treated kinetically and the electrons are treated as a fluid. We discuss briefly the method of calculation described in detail by *Chodura* [1975] and *Sgro and Nielson* [1976], and we discuss thoroughly the initial and boundary conditions used. The code treats all variables as functions of time and of one spatial variable x, the abscissa along the shock normal. The positive x axis points toward the downstream region. The ions are treated as particles and move in the four-dimensional phase space (v_x, v_y, v_z, x). Their motion is solved by the particle in cell technique, the equation of motion of each ion being

$$m_i \frac{d\mathbf{v}}{dt} = e\left(\mathbf{E} + \frac{\mathbf{v}}{c} \times \mathbf{B}\right) + \mathbf{P} \tag{1}$$

$\mathbf{P}$ is a mean friction force, $\mathbf{P} = -e\eta\mathbf{J}$, exerted by the electrons as a macroscopic force only, $\mathbf{J}$ is the current, and η represents a phenomelogical anomalous resistivity, which gives rise to electron Ohmic heating; η is a constant throughout this paper. The ions are initially distributed in phase space as described later and subsequently accelerated by the electromagnetic fields. We thus know the ion distribution function $f_i(x, \mathbf{v}, t)$, and by averaging we find the ion density and ion average velocity

$$n_i = \int f_i(x, \mathbf{v}, t) d^3\mathbf{v} \qquad \mathbf{V}_i = \frac{1}{n_i} \int \mathbf{v}_i f_i(x, \mathbf{v}, t) d^3\mathbf{v}$$

We assume charge neutrality ($n_e = n_i = n$; $V_{ex} = V_{ix} = V_x$) and treat the electrons as a massless fluid. The electron momentum equation is then

$$n_e m_e \frac{d\mathbf{V}_e}{dt} = 0 = -en_e\left(\mathbf{E} + \frac{\mathbf{V}_e}{c} \times \mathbf{B}\right) - \nabla p_e - n_e\mathbf{P} \tag{2}$$

where p_e and $\mathbf{V}_e$ are the scalar pressure and the average velocity of the electrons. In the perpendicular case, the magnetic field $\mathbf{B}$ remains parallel to one direction, chosen to be the z direction. Letting $\mathbf{B} = \nabla \times \mathbf{A}$, the relevant equations of Maxwell are

$$E_y = -\frac{1}{c}\frac{\partial A_y}{\partial t}$$

$$B = \frac{\partial}{\partial x} A_y \tag{3}$$

$$J_y = -\frac{c}{4\pi}\frac{\partial^2}{\partial x^2} A_y$$

These equations are used to rewrite the y component of the electron momentum equation (2)

$$\eta J_y = E_y - \frac{1}{c} V_x B$$

as

$$\frac{c^2\eta}{4\pi}\frac{\partial^2}{\partial x^2} A_y = \frac{\partial A_y}{\partial t} + V_x \frac{\partial A_y}{\partial x} \tag{4}$$

which can then be solved by standard techniques [*Sgro and Nielson*, 1976]. Similarly, the x component of the electron momentum equation (2) gives for E_x

$$E_x = -\frac{1}{c} V_{ey} B - \frac{1}{ne}\frac{\partial p_e}{\partial x} \tag{5}$$

To solve this equation, an electron energy equation is needed:

$$\left(\frac{\partial}{\partial t} + V_x \frac{\partial}{\partial x}\right) p_e = (\gamma_e - 1)\eta J_y^2 - \gamma_e p_e \frac{\partial V_x}{\partial x} \tag{6}$$

where we assume $p_e = n\,KT_e$, and $\gamma_e = 5/3$. An auxiliary variable, not needed in the calculation but useful in the analysis, is the electric potential $\phi(x) = -\int_{-\infty}^{x} E_x\, dx$, which can be expressed, using equation (5) and $V_{ey} = -J_y/ne + V_{iy}$, as

$$e\phi(x) = \int_{\infty}^{x} \frac{1}{n} \frac{\partial}{\partial x'} \left(\frac{B^2}{8\pi} + p_e\right) dx' + \int_{\infty}^{x} \frac{1}{c} V_{iy} B\, dx' \tag{7}$$

In our analysis we will often make use of (1) in the form

$$\frac{d}{dt} v_x = -\frac{e}{m_i} \frac{\partial}{\partial x} \phi + \frac{e}{m_i c} v_y B \tag{8}$$

$$\frac{d}{dt} v_y = -\frac{e}{m_i c} (v_x - V_x) B \tag{9}$$

valid in the limit of small resistivity.

The iterative scheme is as follows: given E_x, E_y, B, and J_y, the ions are moved by using equation (1). The moments n, V_x, V_{iy} are then gathered, and (4) is solved for A_y. Then (3) gives B, J_y, E_y, and $V_{ey} = J_y/ne + V_{iy}$. Finally, (6) gives p_e (or T_e) and (5) gives E_x.

These equations are supplemented by appropriate initial and boundary conditions. Unlike previous shock simulations, we have chosen to initialize the shock without a driving piston. This allows us to eliminate any eventual effect of the driving piston on the shock formation and also to produce a shock at rest in the simulation frame, simplifying the diagnostics. The initial state consists of two uniform regions separated by a thin intermediate layer. In the upstream state (the left region in the simulation), the particle ions are uniformly distributed in x and given random velocities to approximate a Maxwellian distribution convecting toward the intermediate region with appropriate density (n_1), temperature (T_{i1}) and flow speed (V_1) in the x direction. The upstream magnetic field (B_1) and temperature of the fluid electrons (T_{e1}) are also assumed to be uniform. The downstream region is prepared similarly with density (n_2), ion temperature (T_{i2}), flow speed (V_2), magnetic field (B_2), and electron temperature (T_{e2}). The thin intermediate region is prepared such that the density is a linear function of x which matches n_1 at the left end and n_2 at the right end and satisfies $B/B_1 = n/n_1 = V_1/V_x$, some temperature profile being assumed. The downstream quantities are computed from the upstream values using the Rankine-Hugoniot relations with $\gamma = 5/3$ and an assumed initial value of T_{e2}/T_{i2} [*Tidman and Krall*, 1971]. The aim of this method is to prepare at time $t = 0$ a shock transition 'sufficiently' close to the final state so that the system can eventually reach this final state by allowing the shock transition to evolve in time. The initial downstream state is by necessity an approximation. Since there is no ion heating in the z direction in the simulation, the ions evolve two-dimensionally in velocity space, while the fluid electrons behave three-dimensionally. Therefore, the downstream state computed by using Rankine-Hugoniot relations, which assume complete ion thermalization, cannot be reached rigorously. The system is allowed to evolve in time and space subject to the following boundary conditions. Equation (4) is solved keeping the magnetic field B fixed at the boundaries, and (5) is solved assuming $\partial p_e/\partial x = 0$ (or p_e = constant) at the left end. A constant flux $n_1 V_1$ of upstream plasma is maintained at the left end.

While for all cases of interest the upstream ion velocity is much larger than the thermal speed so that no upstream ion has a negative x velocity, the parameter T_{i2}/T_{e2} ($t = 0$) is often large enough for the downstream ion distribution to have a negative x velocity wing. The flux F_l leaving the system at the right end is easily computed as

$$F_l = \int_0^{\infty} v_x f_i(v_x) dv_x = n_2 V_2$$

$$\cdot \left[1 + \frac{1}{2}\left(\frac{\exp(-m_i V_2^2/2KT_{i2})}{\pi^{1/2} V_2 (m_i/2KT_{i2})^{1/2}} - \operatorname{erfc}\left(V_2/(2KT_{i2}/m_i)^{1/2}\right)\right)\right]$$

assuming a Maxwellian for f_i. Particles which exit downstream at the right end are then reinserted into the system such that the upstream flux at the left end is maintained as is the negative x velocity wing at the right end. Then, at each time step a fraction $(1 - n_2V_2/F_l)$ of the particles escaping the system are readmitted into the right end, with negative random x velocities approximating the negative wing of f_i, and the remaining fraction n_2V_2/F_l of ions are injected into the left end. The next flux leaving the system at the right end is thus exactly n_2V_2 and balances the incoming upstream flux at the left end. This implies that the total number of particles is conserved and also that there is no source or sink of mass, momentum, or energy in the system, since downstream and upstream states are related by Rankine-Hugoniot relations. This procedure is accurate as long as the downstream distribution remains Maxwellian, i.e., as long as the perturbations coming from the transition region (shock region) and convected downstream with approximately a velocity V_2 do not reach the right end of the system. In practice, the size of the system is chosen to be large enough for magnetic effects on the ions to be investigated during the time needed for an initial perturbation in the transition region to reach the right end.

3. ANALYSIS OF A TYPICAL CASE

This section is devoted to a detailed study of one particular simulation run, characterized by an Alfvén Mach number $M_A = V_1/(B_1^2/4\pi n_1 m_i)^{1/2} = 6$ and electron and ion upstream beta $\beta_{e1} = \beta_{i1} = 1$. The ratio ω_{pi}/ω_{ci}, where ω_{pi} is the upstream ion plasma frequency and ω_{ci} is the upstream ion gyrofrequency, is taken equal to 7.8×10^3. These values are fairly typical of supercritical bow shocks [*Greenstadt et al.*, 1980]. The resistivity η, taken as constant, is $\eta/4\pi = 1.2 \times 10^{-4}\, \omega_{pi}^{-1}$, which corresponds to a collision frequency $\nu/\omega_{pi} = \eta\omega_{pe}^2/4\pi\omega_{pi} = 0.22$. Such a resistivity is much larger than classical and on the same order of the anomalous resisitivity expected from cross field instabilities [*Davidson and Krall*, 1977]: it is, however, sufficiently small for the density and the magnetic field to be reasonably well coupled. In our discussion, lengths are usually normalized to c/ω_{pi}, times to either ω_{pi}^{-1} or ω_{ci}^{-1}, densities to n_1, average velocities to V_1, magnetic fields to B_1 and electric potentials to $m_iV_1^2/2e$. The total length of the numerical system is 30 c/ω_{pi}, much larger than the upstream ion gyroradius $V_1/\omega_{ci} = M_A c/\omega_{pi} = 6\, c/\omega_{pi}$, and the cell size is taken equal to the resistive scale length $\eta c^2/4\pi V_1 = 0.15\, c/\omega_{pi}$. The initial value of T_{e2}/T_{i2} is chosen such that $\beta_{i2} = \beta_{i1}$, which represents idealized two-dimensional ($\gamma_i = 2$) ion heating. Twenty thousand simulation particles are used in the calculation.

Numerical results are shown in Figures 1–4, which display the normalized $x - v_x$ and $x - v_y$ phase space for the ions and

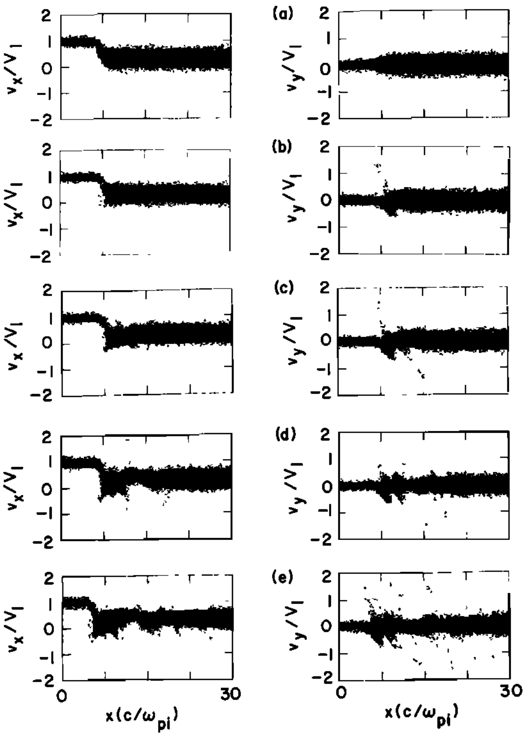

Fig. 1. v_x versus x and v_y versus x phase space for $M_A = 6$, $\beta_{e1} = \beta_{i1} = 1$ at (*a*) $t = 0$, (*b*) 1.3 ω_{ci}^{-1}, (*c*) 2.6 ω_{ci}^{-1}, (*d*) 5.2 ω_{ci}^{-1}, and (*e*) 9.6 ω_{ci}^{-1}.

profiles of magnetic field, density, and electric potential at five different times: 0, 1.3, 2.6, 5.2, and 9.6 ω_{ci}^{-1}. The initial shock transition, shown in Figures 1–4*a*, is out of balance, since plasma and field quantities do not satisfy Rankine-Hugoniot relations in this intermediate region. As the system is allowed to evolve in time, the intermediate region steepens until its width reaches the resistive length. At the same time some of the downstream ions, which initially have negative x velocities due to the large initial downstream ion temperature (Figure 1*a*), flow upstream and are accelerated in the potential hill, gaining an energy $e\Delta\phi$. In addition, these ions undergo a large acceleration in the positive y direction because for these particles the electric force $eE_y \simeq eV_1B_1/c \simeq eV_xB/c$ does not cancel the magnetic force ev_xB/c (*Auer et al.* [1971], *Biskamp and Welter* [1972], *Sherwell and Cairns* [1977]; paper 1). The escaping ions form a foot region (Figures 2*b*, 3*b*), since their density adds to the incoming ions density. Simultaneously, an overshoot appears in the potential (Figure 4*b*), caused by the large y velocities of the escaping ions which now contribute significantly to the second term of the right-hand side (7). A self-sustaining reflection process is then initiated (paper 1). The presence of the escaping ions shifts the rest frame of the incoming stream in the foot region, and the average ion x velocity V_x is somewhat smaller than the v_x of an incoming ion. As a result, some magnetic deflection occurs in the foot region (equations (8) and (9)), which, together with the electric potential, can 'reflect' some of the incoming ions. Note that at this time the hot downstream ions can no longer escape upstream because of the electric potential overshoot. The source of reflected gyrating ions thus changes qualitatively in less than a gyrotime ω_{ci}^{-1} from downstream to upstream ions. This behavior has been checked to be independent of the initial conditions. When the initial downstream temperature ratio T_{e2}/T_{i2} is chosen very small, many downstream ions can initially escape upstream, but they build up a potential overshoot sufficient to prevent other downstream particles from following the same trajectories. When T_{e2}/T_{i2} (t = 0) is large, there are no downstream ions with $v_x < 0$. In this case the intermediate region steepens up, causing the ions in this region to be heated with approximately $\gamma_i = 2$, which produces some ions with negative v_x, and the same process can take place. The same resulting behavior was also obtained with an initial step function discontinuity between upstream and downstream regions instead of a finite transition layer.

Figures 1–4*c* show the results at $t = 2.6\ \omega_{ci}^{-1}$, by which time the system has forgotten the initial conditions. The reflected ions have gained enough energy, owing to the E_y acceleration, to overcome the potential barrier when they come back to the shock front and gyrate downstream (compare $x - v_x$ and $x - v_y$ phase space in Figure 1*c*). Overshoots in magnetic field and density appear, followed by undershoots, the scales of which are clearly related to the ion gyroradius of the gyrating stream, about 3–4 c/ω_{pi}. The magnetic field and density profiles are very similar. The foot region is about 2 c/ω_{pi} wide (Figure 1*c* and 2*c*), which is smaller than the upstream gyroradius $V_1/\omega_{ci} = 6\ c/\omega_{pi}$. This is related to the fact that in the foot region, reflected ions have small negative x velocities, reaching at most 1/2 V_1 in absolute value, because the reflected ions convert most of the energy which they gain coming down the potential hill into y velocity. Reflected ions have positive values of v_y up

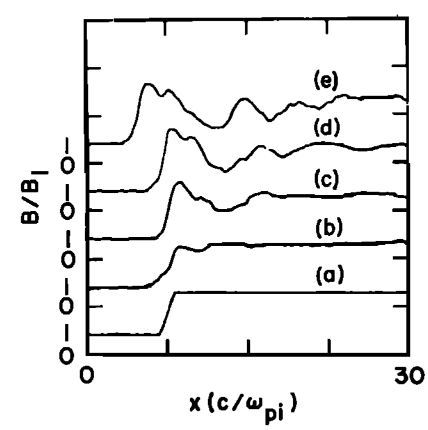

Fig. 2. Magnetic field profiles for $M_A = 6$, $\beta_{e1} = \beta_{i1} = 1$ at the same times as in Figure 1.

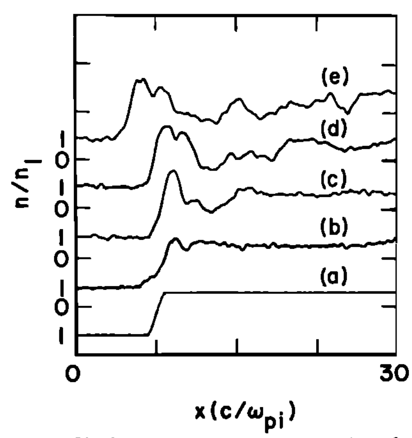

Fig. 3. Density profile for $M_A = 6$, $\beta_{e1} = \beta_{i1} = 1$ at the same times as in Figure 1.

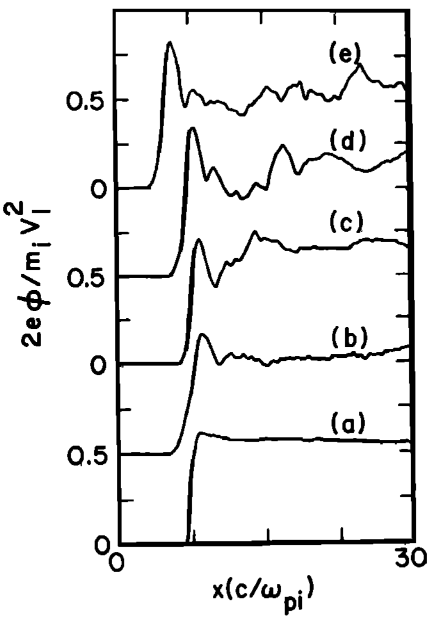

Fig. 4. Electric potential profile normalized by $m_i V_1^2/2e$ for $M_A = 6$, $\beta_{e1} = \beta_{i1} = 1$ at the same times as in Figure 1.

to about 1.6 V_1 in the foot region, where ϕ is approximately zero. The excess energy compared with the upstream kinetic energy is due to the net positive work done by E_y on these particles.

It is worth noting the importance of the foot region for particle dynamics in the shock. The foot region acts as a brake for the incoming ions, both electrostatically and magnetically. The electrostatic part has already been discussed (overshoot in potential due to deflection in the y direction of the reflected ions) and constitutes the main contribution in the present case. The potential reaches 0.8 times the average upstream kinetic energy, which is enough to reflect a significant fraction of the upstream ions. The magnetic part is the deflection due to the shift of the ion plasma frame, as explained in paper 1. Although not very significant for the present case, it can be seen in Figure 1*c* that the incoming ions acquire negative y velocities in the foot region, which necessarily results in some x deceleration (equation (8)). The respective importance of the magnetic part with respect to the electrostatic part increases with M_A, as discussed in the next section.

Figures 1*d* and 1*e* show $x - v_x$ and $x - v_y$ phase space at $t = 5.2$ and $9.6\ \omega_{ci}^{-1}$. The reflected ions continue to gyrate downstream with a guiding center velocity approximately equal to V_2. In addition, the compressions and rarefactions in the density and magnetic field are produced dynamically by the gyrating stream as is evident from comparing Figure 1*e* and Figure 3*e*. The latter is consistent with earlier simulations [*Biskamp and Welter,* 1972] and the discussion of *Morse* [1976]. The first revolution of the gyrating stream behind the shock front is altered by the presence of the potential overshoot (paper 1), which acts as a barrier between the downstream and upstream region. The gyrating stream, starting from the foot region, would have come back after a complete revolution significantly closer to the magnetic ramp in the absence of the potential overshoot. Instead, the turning point of the gyrating stream is slightly further downstream, resulting in the appearance of the second reduced maximum in the magnetic field and density overshoots (Figures 2*e* and 3*e*). The first maximum is due to the incoming ions, some of which pile up at the shock front before being reflected or continuing downstream. Thus the overshoots in the magnetic field and density are extended and are significantly longer than that of the potential (Figures 2–4*e*)).

The ions that are transmitted downstream through the shock front without reflection are adiabatically heated, as determined from the velocity spread in phase space (Figure 1*e*). However, the 'temperatures' in both the x and y directions are not constant just behind the shock transition (i.e., for several ion gyroradii of the gyrating ions (Figure 1*e*)) but smooth out further downstream. One notes in particular that phase mixing between the ions transmitted downstream with and without reflection is not very efficient. The gyrating stream pattern remains easily visible even after several ion gyroradii (Figure 1*e*), although the gyrating stream progressively loses some kinetic energy, from about 3.2 times the upstream kinetic energy just behind the shock front to about 1.7 at $x = 25\ c/\omega_{pi}$. The energy goes primarily into heating up the bulk of the transmitted ions. This coupling between the gyrating stream and transmitted core has been found not to be due to the anomalous transfer term in the ion equation of motion, equation (1).

Figure 5 shows β_e and β_i as a function of x at $t = 9.6\ \omega_{ci}^{-1}$. β_i is defined as the $x - x$ component of the ion pressure tensor divided by the local magnetic pressure. β_i achieves large values both in the front (~9) and also just behind the shock front (~11). Of course, these large values of β_i do not represent actual ion temperatures, but rather a large separation in velocity between the reflected and transmitted ions. The value of β_i farther downstream ($x = 20\ c/\omega_{pi}$) is about 2.5, significantly larger than the value of β_i expected from ion compressional heating with $\gamma_i = 2$ (compare with the $\beta_i \simeq 1$ of the remnant of initial downstream plasma at $x \simeq 30\ c/\omega_{pi}$

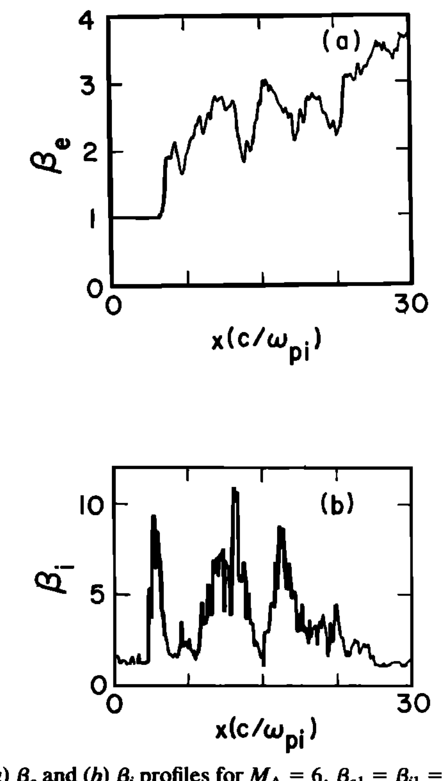

Fig. 5. (*a*) β_e and (*b*) β_i profiles for $M_A = 6$, $\beta_{e1} = \beta_{i1} = 1$ at $t = 9.6\ \omega_{ci}^{-1}$.

in Figure 1*e*). The value of β_e is also significantly larger than unity because of resistive heating; β_e is about 2.7 at $x = 20\ c/\omega_{pi}$.

In Figure 6 are plotted V_x/V_1, V_{iy}/V_1, and V_{ey}/V_1 as functions of x. A comparison of Figure 3*e* and Figure 6 shows that the flux nV_x is approximately constant. Although V_{ey} is large (0.5 V_1) at the shock front, the current in the y direction is not very strong because there is also a net ion drift in the y direction, attaining a maximum of 0.35 V_1 at the shock front. These large ion y velocities have also been found in the simulations of *Auer et al.* [1971]. In the simulation presented in this section, the magnetic ramp is as wide as the foot region ($\sim c/\omega_{pi}$), leading to a rather weak y current. As shown in the next section, the use of a larger number of cells and smaller resistivity would make clear the separation between ion scales (foot region) and the resistive scale on which B increases up to its maximum (ramp region).

Figure 7 presents a time history of three quantities: the maxima, ϕ_{max} and B_{max}, of electric potential and magnetic field in their respective overshoots and the percentage of reflected ions α. This percentage is computed as the flux in the x direction of ions with negative x velocities on the left of the shock front, defined as where the potential reaches its maximum, normalized by the upstream flux n_1V_1. These quantities are shown between 2 ω_{ci}^{-1}, after which time the system has essentially forgotten its initial conditions, and the final time $t = 9.6\ \omega_{ci}^{-1}$. The system behaves fairly steadily, as can be inferred from the small relative standard deviations around the average values of the measured quantities reported in Table 1.

The quasi-stationary behavior of this hybrid model simulation is in contrast with the results of *Biskamp and Welter* [1972], obtained with a one-dimensional particle code, who have observed a periodically vanishing leading edge of the shock. We have performed runs in which the shock behavior is less steady than in the case discussed here (see next section) without recovering their results, however. According to *Biskamp* [1973], the reflected ions in the foot region of the particle simulation pile up when they reach their turning point ($v_x = 0$) and therefore produce a local increase of density, large enough to reflect other particles, and so on. The discrepancy between particle and hybrid simulations may be due to the fact that a larger number of ions are reflected in the dissipationless particle code than in the hybrid code. This excess of reflected ions could explain the large local increase of the density in the foot region described by *Biskamp* [1973].

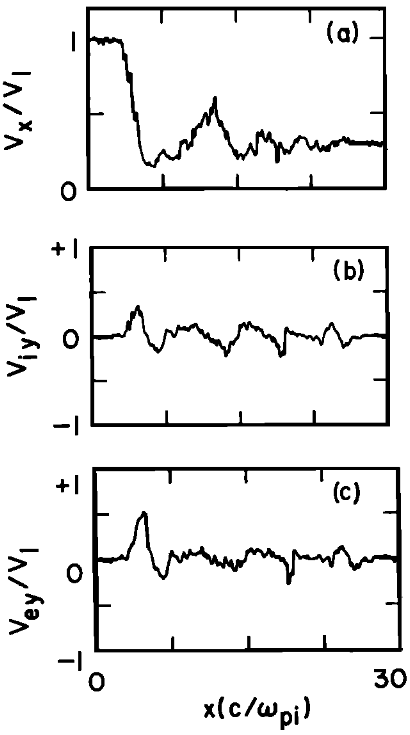

Fig. 6. (*a*) V_x, (*b*) V_{iy} and (*c*) V_{ey} profiles for $M_A = 6$, $\beta_{e1} = \beta_{i1} = 1$ at $t = 9.6\ \omega_{ci}^{-1}$.

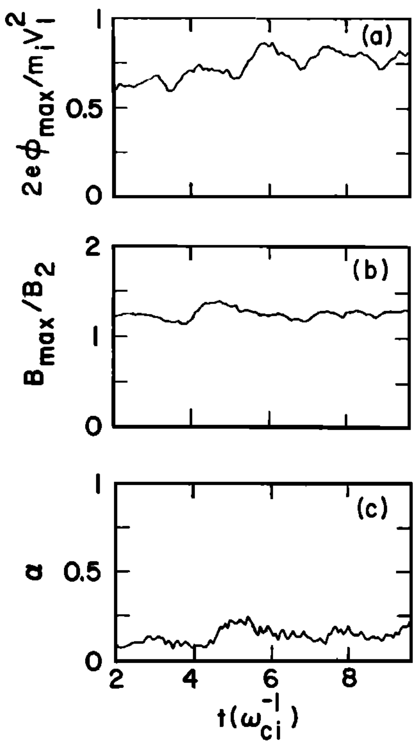

Fig. 7. Time histories of (*a*) ϕ_{max}, (*b*) B_{max}, and (*c*) α, between $t = 2\ \omega_{ci}^{-1}$ and $t = 9.6\ \omega_{ci}^{-1}$.

We note also that in our simulations the shock front remains almost immobile, which indicates that the shock is in mass, momentum, and energy balance. The shock front actually moves slightly towards the left (Figure 1) between $t = 5.2\ \omega_{ci}^{-1}$ and $t = 9.6\ \omega_{ci}^{-1}$ but does not oscillate as suggested by *Morse* [1976]. The downstream magnetic field, density, x and y average velocities reach their expected Rankine-Hugoniot values to within 20% (see, for example Figures 2, 3 and 6*b*). The sum of β_e and β_i is about 5.2 at $x = 20\ c/\omega_{pi}$ (Figure 5), in reasonable agreement with the Rankine-Hugoniot value 4.2. However, care should be exercised in providing the proper interpretation for β_i as discussed previously.

TABLE 1. Average Value and rms Deviation of the Magnetic Field and Potential Overshoot and the Number of Reflected Ions for the Run Described in Section 3

	Average Value	RMS Deviation
B_{max}/B_2	1.26	0.06
$2e\phi_{max}/m_iV_1^2$	0.76	0.06
α(%)	13.7	4.0

4. PARAMETER STUDIES

In this section, we discuss the scaling of various properties of the shock structure with the parameters of the model, i.e., the resistivity η, the upstream plasma β parameters β_{e1} and β_{i1}, and the upstream Alfvén Mach number M_A. We have investigated these upstream parameters in ranges typically observed in the bow shock of the earth and other planets, i.e., $\beta_{i1} \simeq 0.1$–1, $\beta_{e1} \simeq 0.1$–1, $M_A = 2$–20 [*Greenstadt and Fredricks*, 1979; *Russell et al.*, 1981; *Eselevich*, 1981]. We have not attempted to discuss our results in terms of the magnetosonic Mach number $M_S = V_1/(V_{A1}^2 + C_{s1}^2)^{1/2}$, where V_{A1} and C_{s1} are the upstream Alfvén and sound speeds, because the MHD concept of fast magnetosonic shock wave has little relevance for the highly kinetic, supercritical situation usually observed in the bow shock. We conclude this section with a discussion of the transition between the low Mach number, MHD regime, and the supercritical regime for which ion reflection becomes important (lower critical Mach number M_A^*). We also discuss the possible existence of an upper critical Mach number M_A^{**}, defined as the transition between the supercritical regime and a regime for which no shock solution exists.

a. *Resistivity and Electron Heating*

The resistivity expected in the earth's bow shock is due to collisionless wave particle interactions driven by field gradients [*Wu*, 1982]. We have explored a wide range of resistivities from $\eta/4\pi = 3 \times 10^{-6}\ \omega_{pi}^{-1}$ to $6 \times 10^{-4}\ \omega_{pi}^{-1}$, which are typical of current driven instabilities [*Davidson and Krall*, 1977]. Figure 8 shows the magnetic field profiles for $M_A = 6$, $\beta_{e1} = \beta_{i1} = 1$ and $\eta\omega_{pi}/4\pi = 3 \times 10^{-6}, 3 \times 10^{-5}, 1 \times 10^{-4}, 6 \times 10^{-4}$. We note that, except for the case of highest resistivity, the structure of the magnetic field profile remains relatively invariant, always exhibiting a foot region, a magnetic ramp, and an overshoot (Figure 8). However, the separation of the various physical scales associated with these regions becomes clearer as η decreases. The foot region is associated with the reflected ions and scales as c/ω_{pi} independently of η, whereas the magnetic ramp scales with the resistive length and becomes thinner as η decreases.

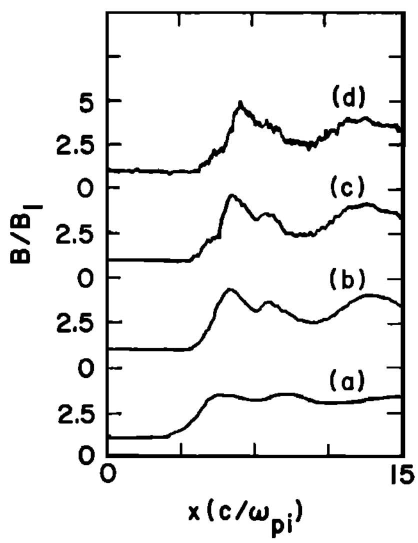

Fig. 8. Magnetic field profiles for $M_A = 6$, $\beta_{e1} = \beta_{i1} = 1$, $t = 2.6\ \omega_{ci}^{-1}$ with (*a*) $n\omega_{pi}/4\pi = 6 \times 10^{-4}$, (*b*) 10^{-4}, (*c*) 3×10^{-5}, and (*d*) 3×10^{-6}.

TABLE 2. Values of Potential and Magnetic Field Overshoots, Number of Reflected Ions and Electron Beta as a Function of resistivity for $M_A = 6$, $\beta_{e1} = \beta_{i1} = 1$

$\eta/4\pi\ (\omega_{pi}^{-1})$	$2e\phi_{max}/m_iV_1^2$	α	β_e'	B_{max}/B_2
3×10^{-6}	0.55	23	0.5	1.5
3×10^{-5}	0.70	20	0.6	1.4
1×10^{-4}	0.75	15	1.1	1.3
6×10^{-4}	0.80	10	2.5	1.0

For $\eta/4\pi = 6 \times 10^{-4}\ \omega_{pi}^{-1}$, the magnetic field diffuses enough through the plasma to destroy the overshoot structure and to appear as a smooth monotonic transition.

The maximum of electric potential and magnetic field in their respective overshoots, the number of reflected particles α, and the electron beta just beyond the magnetic ramp β_e' are given in Table 2 for the different resistivities. The sensitivity to η of these quantities, although noticeable, remains weak. When η varies by a factor 200, β_e' varies by a factor 5, α by a factor 2.3, ϕ_{max} by 1.45 and B_{max} by 1.5. Moreover, most of the variation occurs close to the highest value of η for which the overall structure of the shock is strongly modified. The decrease of the field overshoot is not surprising, since the resistivity tends to smooth out the magnetic field profile. β_e' increases with η, which implies an increase in the resistive electron heating. As a result, ϕ_{max} also tends to increase with η (equation (7)). However, this increase of ϕ_{max} does not lead to an increase of α, since α decreases with increasing η (Table 2), implying that magnetic deflection becomes less effective with respect to electrostatic deceleration as η increases.

The fact that shock quantities are weakly dependent on resistivity may be understood by the following order of magnitude estimate. If we consider a steady state situation, the electron energy equation (6) in its entropy form is approximately

$$\left[\frac{1}{\gamma_e - 1}\right][V_x^{-(\gamma_e-1)}]\,\frac{\Delta(p_eV_x^{\gamma_e})}{\Delta x} \simeq \eta\left(\frac{c}{4\pi}\right)^2\left(\frac{\Delta B}{\Delta x}\right)^2 \qquad (10)$$

If we take for Δx the resistive length $L_r = c^2\eta/4\pi V_1$ (the shortest scale of the system), estimate V_x and B behind the main magnetic ramp as V_2 and B_2, and approximate $V_x^{\gamma_e-1} \simeq (V_1/2)^{\gamma_e-1}$, equation (10) gives the electron pressure behind the magnetic ramp

$$p_e' \simeq \left(\frac{V_1}{V_2}\right)^{\gamma_e}\left[\frac{1}{4\pi}(B_2 - B_1)^2\,\frac{\gamma_e - 1}{2^{\gamma_e-1}} + p_{e1}\right]$$

or, with $V_1/V_2 = B_2/B_1 \simeq 4$ and $\gamma_e = 5/3$,

$$\beta_e' \simeq 4.7 + 0.6\,\beta_{e1} \qquad (11)$$

Equation (11) is of course only an order of magnitude estimate (compare (11) and Table 2). Nevertheless, the absence of η in (11) explains the weak dependence on η of our results. Furthermore, β_e' given by (11) is independent of M_A. Consequently, the amount of energy going to the electrons by Ohmic heating cannot be increased indefinitely with M_A. Such a conclusion has also been suggested by electron heating measurements in laboratory experiments [*Paul et al.*, 1967; *Phillips and Robson*, 1972]. It must be pointed out, however, that although the estimate of (11) is rather satisfactory (as far as its M_A dependence is concerned) just behind the main magnetic ramp, it becomes inaccurate when considering the jump in β_e between the far downstream and upstream regions. In particular, for $M_A > 8$, the magnetic field profile is highly distorted, which causes additional Ohmic dissipation far behind the magnetic ramp. These results are shown in Table 3, which displays the values of β_e just behind the ramp (β_e') and far downstream as a function of M_A for $\beta_{e1} = 0.01$, $\beta_{i1} = 1.$, $\eta/4\pi = 10^{-4}\ \omega_{pi}^{-1}$ at $t = 2.6\ \omega_{ci}^{-1}$.

b. Upstream Electron Temperature β_{e1}

From the same equation (11) one would also expect the upstream electron temperature not to play a significant role for the shock structure. As long as β_{e1} does not exceed about 3, the electron heating is dominated by Ohmic friction. We have checked numerically that varying β_{e1} from 0.1 to 1 in two typical cases ($M_A = 6$, $\beta_{i1} = 0.1$ and $M_A = 6$, $\beta_{i1} = 1$) produces less than 10% variation of the magnetic field and the ion and electron bulk velocities. We note that the value of β_e' is 1.7 for the case with $\beta_{e1} = 1$ investigated in section 3 (Figure 5). On the other hand, Table 3 gives $\beta_e' = 1.1$ for nearly the same case as in section 3 except that β_{e1} is 0.01 instead of 1. This increase of β_e' with β_{e1} is in good agreement with the estimate of (11). We have also verified that adiabatic heating is dominant for large β_{e1}. β_e actually decreases from upstream to downstream for $\beta_{e1} = 10$ ($M_A = 6$, $\beta_{i1} = 1$, $\eta/4\pi = 10^{-4}\ \omega_{pi}^{-1}$) owing to the fact that $\gamma_e\ (= 5/3)$ is slightly less than 2.

c. Upstream Alfvén Mach Number M_A

Numerical runs for $M_A = 4, 6, 8, 10$ and $\beta_{e1} = \beta_{i1} = 1$ have been performed in order to investigate the M_A dependence of the shock structure. The resistivity has been taken proportional to M_A, so that the resistive length $L_r = \eta c^2/4\pi V_1$ remains constant and equal to 0.13 c/ω_{pi} ($\eta/4\pi = 10^{-4}\omega_{pi}^{-1}$ for $M_A = 6$). Figure 9 shows the magnetic field profiles as a function of x corresponding to these four cases at a time $t = 10.2\ \omega_{ci}^{-1}$. The abscissa for each of these profiles has been normalized by V_1/ω_{ci2}, where ω_{ci2} is the ion gyrofrequency computed by using the downstream magnetic field. Figure 9 shows that the shapes of the profiles are very similar, the only significant difference being that the magnitude of the variations of the field becomes larger as M_A increases. In addition, the figure shows that the scales of the field features are very much alike, and in particular that the width of the magnetic field overshoot is roughly equal to 3 V_1/ω_{ci2}. The scaling with V_1/ω_{ci2} can be understood qualitatively as follows. The ion gyrating stream dynamically shapes the density profile, and hence the magnetic field profile, since n and B are strongly coupled. Therefore, we expect the gyroradius of the gyrating stream to be the relevant length scale in the post magnetic ramp region. Such a gyroradius should be computed by using the downstream magnetic field, which explains ω_{ci2}; what remains to be shown is that the magnitude of the gyrating stream velocity scales as V_1. Consider the idealized case of a shock front

TABLE 3. Electron Beta Behind the Ramp and Far Downstream as a Function of Mach Number

M_A	4	6	8	10
β_e' (ramp)	0.5	1.1	1.	1.3
β_e (far downstream)	1	2.5	5.	9

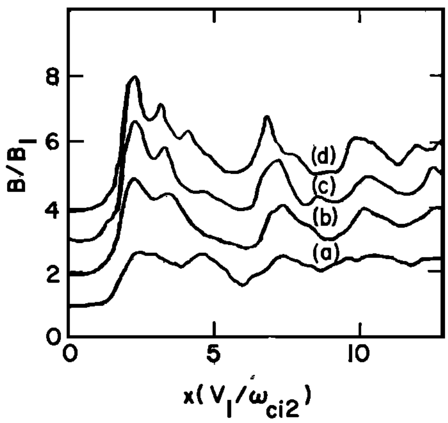

Fig. 9. Magnetic field profiles for $\beta_{e1} = \beta_{i1} = 1$, $t = 10.2\ \omega_{ci}^{-1}$ (*a*) with $M_A = 4$, (*b*) 6, (*c*) 8, and (*d*) 10. The x abscissa has been normalized by V_1/ω_{ci2}.

behaving as a pure reflecting wall. The trajectory in uniform $E_y = V_1B_1/c$ and B_1 of an incoming test ion, reflected at the shock front with $v_x = -V_1$, $v_y = 0$, can easily be computed and gives the result that the test ion comes back to the shock front after half a revolution with $v_x = 1.64\ V_1$, $v_y = 1.90\ V_1$. Its kinetic energy, 6.3 ($m_iV_1^2/2$), would then be large enough to be nearly unaffected by the crossing of the potential barrier, since $e\phi_{max} < \frac{1}{2}m_iV_1^2$, and this test particle would gyrate downstream with a velocity scaling as V_1. Of course, the exact ion dynamics in the foot and ramp regions make the actual picture much more complicated. Nevertheless, the simulations reveal that the gyrating reflected ions acquire a kinetic energy equal to 3–3.5 times $m_iV_1^2/2$ just beyond the main magnetic ramp (see, for example, Figure 1*e*) rather independently of the Mach number. The V_1/ω_{ci2} scaling of the magnetic field features in the downstream region was first proposed by *Morse* [1976] on the basis of qualitative arguments which, however, did not include the concept of reflected gyrating ion stream.

Figure 10 shows the dependence on M_A of the magnetic field and electric potential overshoots, and number of reflected ions. Plotted are the time averages of α and the maxima of B and ϕ; the error bars indicate the standard deviations for each average. The averaging period, $2\ \omega_{ci}^{-1} \le t \le 10.2\ \omega_{ci}^{-1}$, is chosen to exclude the initial transients in the simulations.

The most important fact revealed by Figure 10 is that there is a direct relation between the number of reflected ions and the size of the magnetic field overshoot: the time averages $\langle\alpha\rangle$ and $\langle B_{max}\rangle$ both increase with M_A in a similar fashion. Moreover, when $\langle\alpha\rangle$ goes to zero, the field overshoot vanishes. As the Mach number increases, the values of $\langle\alpha\rangle$ and $\langle B_{max}\rangle$ approach upper limits, suggesting some sort of saturation mechanism for large M_A, which will be discussed later. The value obtained for $M_A = 8$, $\langle B_{max}\rangle/B_2 = 1.35$ is significantly smaller than the value 1.7 found in the case investigated in paper 1, due to the use in the present paper of a much larger resistivity (section 4*a*)). The variation of $\langle\alpha\rangle$ with M_A may be compared with similar results in the unmagnetized ion analysis of *Chodura* [1975]. We find somewhat higher values of α, especially for $M_A < 10$ ($\alpha \simeq 5\%$ and 18% for $M_A = 6$ and 10 in Chodura's analysis, whereas $\langle\alpha\rangle \simeq 13\%$ and 21% in ours). Furthermore, the difference is enhanced as the

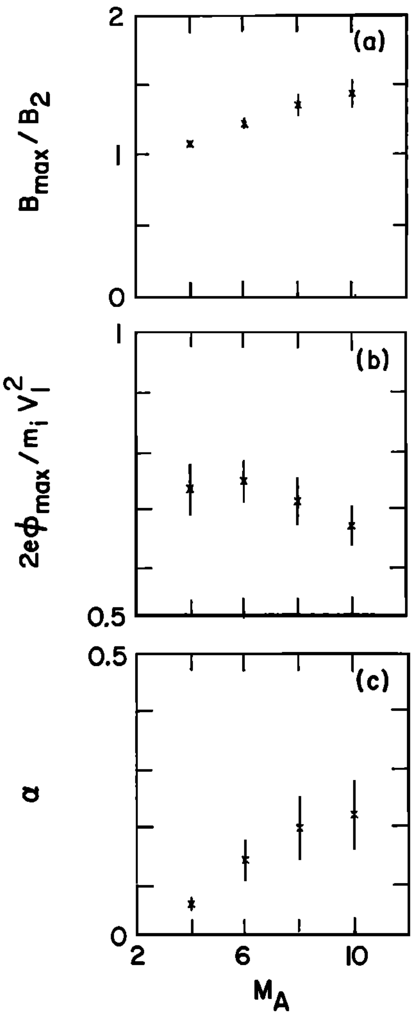

Fig. 10. (*a*) B_{max}, (*b*) ϕ_{max}, and (*c*) α as functions of M_A for $\beta_{e1} = \beta_{i1} = 1$. Crosses are time averages. The length of the vertical lines is twice the rms deviation.

resistivity is decreased: $\alpha \simeq 32\%$ for $M_A = 10$, $\eta/4\pi = 10^{-5}$ ω_{pi}^{-1}.

We attribute this difference to the importance of magnetic effects in the dynamics. We note from Figure 10 that the normalized $\langle\phi_{max}\rangle$ goes through a maximum of 0.74 for $M_A = 6$ and then decreases for $M_A > 6$. This result, together with the corresponding variation of α with M_A, can be used to investigate the role of magnetic deflection in the reflection process. For this purpose we evaluate the fraction α' of incoming particles that should be reflected by the potential $\langle\phi_{max}\rangle$ if the ions had only 1 degree of freedom, along the x axis, i.e.,

$$\alpha' = \int_{-\infty}^{V_0} f_{i1}(v_x)dv_x \bigg/ \int_{-\infty}^{+\infty} f_{i1}(v_x)dv_x$$

where f_{i1} is the upstream ion distribution function (Maxwellian) and V_0 is the largest x velocity that leads to reflection, $V_0 = (2e\langle\phi_{max}\rangle/m_i)^{1/2}$. The value of α' is little modified if we calculate α' as a flux ratio instead of a density ratio. The expression giving α' may be reduced to

$$\alpha' = \frac{1}{2}\,\mathrm{erfc}\left[\frac{M_A}{(\beta_{i1})^{1/2}}\left(1 - \frac{V_0}{V_1}\right)\right]$$

The values of $\langle\alpha\rangle$ and α' are listed in Table 4. It is clear from these values that magnetic deflection plays an increasing role with M_A for $M_A \geq 6$, since $\langle\alpha\rangle - \alpha'$ is positive and becomes larger with M_A for $M_A \geq 6$. Table 4 shows also that $\langle\alpha\rangle$ is significantly less than α' for $M_A = 4$, which is rather unexpected, since the only effect of magnetic deflection, if any, should be to add to the electrostatic braking and therefore reflect more particles than in the electrostatic case. This apparent discrepancy is explained as follows. The potential overshoot is observed to be small in the simulation for $M_A = 4$ and $\beta_{i1} = 1$, essentially because $\langle\alpha\rangle$ is small. Furthermore, the top of the potential overshoot is flattened by thermal effects, which are significant in this case because the upstream ion thermal velocity becomes comparable to the upstream bulk speed. As a result, a relatively wide ($\sim c/\omega_{pi}$) region of the potential overshoot has a small derivative $\partial\phi/\partial x$. In the reflection process, some of the incoming ions, approximately α' in number, are stopped by the potential barrier, but most of them see their x velocity change sign in the neighborhood of the maximum of ϕ where $\partial\phi/\partial x$ is small (but positive). Such an ion, when reflected, is accelerated in the positive y direction (equation (9)). The term ev_yB/m_ic in equation (8) can then easily exceed the weak term $-\partial\phi/\partial x$ in such a way that the particle eventually surmounts the potential barrier. In other words, most of the α' ions do not have time to go down the potential hill and be recognized as a 'reflected ion' by the diagnostic in the simulation. Rather, they undergo a small loop close to the top of the potential overshoot and gain enough energy by E_y to eventually overcome the potential barrier and convect downstream, where they become indistinguishable from truly 'transmitted' ions.

Finally, we note that although some fluctuations in $\alpha(t)$, $B_{max}(t)$, etc., are noticeable (see rms standard deviations in Figure 10), and, particularly in the high Mach number regime, they remain fairly small. For example, B_{max} varies by less than 7% around its averaged value. Thus the shock structure may be characterized as being quasi-stationary.

d. *Upstream ion β_{i1}*

It is shown for the case investigated in section 3 ($M_A = 6$, $\beta_{i1} = 1$) that regardless of the initial value of T_{e2}/T_{i2}, compressional heating in the early transitory stage of the calculation is sufficient to provide a seed population of downstream ions with negative x velocities. This population leads to a steady stream of reflected ions. However, this scheme is only possible for sufficiently large β_{i1}, since compressional heating is negligible in the limit of small β_{i1}.

We can estimate roughly the limit of β_{i1} (say $\beta_{i1}{}^*$) above which the process is operable, as follows. Compressional heating will produce a significant amount of downstream ions with negative x velocities if

$$v_{thi2} \simeq V_2 \qquad (12)$$

TABLE 4. Percentage of Reflected Ions With $\langle\alpha\rangle$ and Without (α') Magnetic Effects as a Function of Mach Number for $\beta_{e1} = \beta_{i1} = 1$

M_A	4	6	8	10
α, %	5.3	13	18	21
α', %	22	12	3	0.4

The α' are computed by using the values of $<\phi_{max}>$ shown in Figure 10.

where v_{thi2} is the downstream ion thermal velocity. Compressional heating with $\gamma_i = 2$ gives $v_{thi2} = v_{thi1}(n_2/n_1)^{1/2}$, so that equation (11) becomes, using $n_2V_2 = n_1V_1$ and the definitions of β_{i1} and M_A,

$$\beta_{i1}^* = M_A^2(n_2/n_1)^{-3} \tag{13}$$

For $M_A = 6$ and $n_2/n_1 \simeq 4$, equation (13) gives $\beta_{i1}^* \simeq 0.5$. Runs with $\beta_{i1} > \beta_{i1}^*$ have been described earlier. We have, in addition, performed numerical runs with $\beta_{i1} < \beta_{i1}^*$ with the same parameters as in section 4*c* but with $\beta_{i1} = 0.1$ and $\beta_{e1} = 0.1$. The results exhibit somewhat different characteristics with respect to their large β_{i1} counterparts, especially for high M_A, $M_A \geq 8$. The behavior of the shock structure is no longer nearly stationary, but becomes dynamic. However, the main characteristics of the shock structure (foot, ramp, overshoot) remain the same as before: once set up, the overshoots in magnetic field, density, and electric potential persist in time but oscillate in magnitude more, as shown in Figure 11 for $M_A = 10$.

This dynamic behavior may be described qualitatively as follows. Suppose that initially no reflected ions exist. Then the interface between upstream and downstream streams steepens up, although limited by magnetic field diffusion, and enhances the electron heating (note that the estimate of electron heating in equation (11) is no longer valid in the unsteady state considered here). This heating in turn increases the electric potential (equation (7)) so that some ions are reflected. The foot, then formed, smooths out the gradients of density and magnetic field, reducing the electron heating and electric potential, and hence the number of reflected ions. The process then repeats itself. This approximate scheme ignores magnetic effects, which also play a significant role in the reflection process.

Figure 12 shows the same quantities $\langle\alpha\rangle$, $\langle B_{max}\rangle/B_2$, and $2e\langle\phi_{max}\rangle/m_iV_1^2$ and their standard deviations as in Figure 10 for $\beta_{i1} = \beta_{e1} = 0.1$. Again, $\langle\phi_{max}\rangle$ decreases with M_A, which confirms the previous conclusion that magnetic deflection plays an increasing role with M_A. It is interesting to note that the functions $\langle\alpha\rangle$ (M_A) and $\langle B_{max}\rangle$ (M_A) are roughly the same as in Figure 10; i.e., in the time average, the magnetic field overshoot and the number of reflected ions do not depend sensitively on the upstream ion temperature. The magnitudes of the time variations of α, B_{max}, and ϕ_{max}, however, are significantly larger for $\beta_{i1} = 0.1$ than for $\beta_{i1} = 1$ (compare Figure 10 and Figure 12). In particular, for $M_A > 8$ and $\beta_{i1} = 0.1$, the rms value of $\alpha(t)$ becomes comparable to $\langle\alpha\rangle$. The time history of α (Figure 11 for $M_A = 10$) reveals that $\alpha(t)$ is an oscillatory function that vanishes periodically in time with a period of approximately ω_{ci}^{-1}. Thus the ions are reflected dynamically in bunches, instead of continuously.

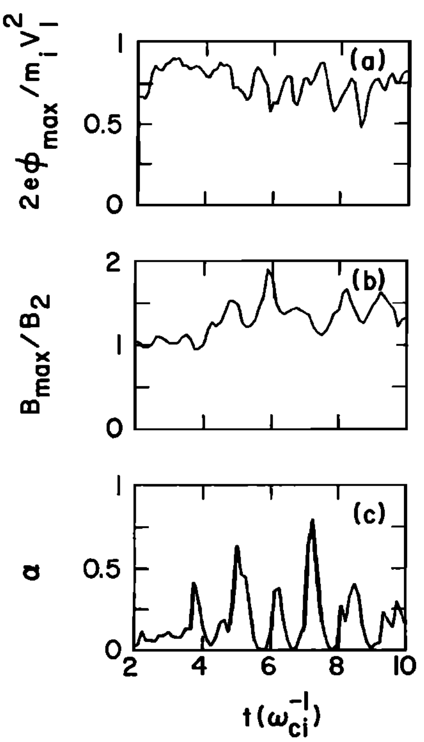

Fig. 11. Time histories of (*a*) ϕ_{max}, (*b*) B_{max}, and (*c*) α between $t = 2\omega_{ci}^{-1}$ and $10.2\ \omega_{ci}^{-1}$ for $\beta_{i1} = 0.1$, $M_A = 10$.

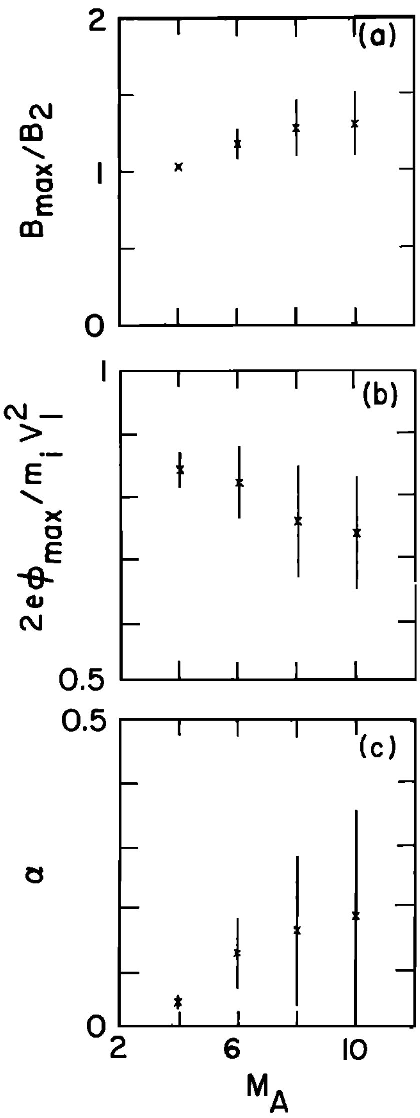

Fig. 12. (*a*) B_{max}, (*b*) ϕ_{max}, and (*c*) α as functions of M_A for $\beta_{i1} = \beta_{e1} = 0.1$.

e. The Critical Mach Numbers

So far, we have investigated a range of M_A typical for the earth and planetary bow shocks ($M_A \simeq$ 4–10). However, low M_A shocks, although unfrequently observed, can occur in the earth bow shock [*Greenstadt and Fredricks,* 1979], and rather high M_A shocks are likely to be observed in the neighborhood of remote planets like Jupiter [*Russell et al.*, 1981]. It is thus worthwhile to investigate the limits of our model for very low and very high Mach numbers.

Low M_A regime and lower critical Mach number M_A.* It is well known [*Tidman and Krall*, 1971] that below a certain critical Mach number M_A^*, the shock behavior is satisfactorily described by fluid theory. Above M_A^*, ion reflection occurs and the shock is called supercritical. The value of M_A^* is given by fluid theory as the Mach number for which $V_2 = C_{s2}$, where C_{s2} is the downstream sound speed $C_{s2}^2 = (\gamma_e T_{e2} + \gamma_i T_{ix2})/m_i$ and T_{ix2} is the x-x component of the ion pressure tensor divided by density. Our simulations are in good agreement with fluid theory, in that when $V_2 > C_{s2}$, no ion reflection occurs ($M_A < M_A^*$) and the opposite for $V_2 < C_{s2}$ (some slight deviations from this behavior, however, are found for high resistivity). For example, M_A^* is found to be between 2.5 and 3 for $\beta_{i1} = \beta_{e1} = 0.01$ in our simulations, in good agreement with fluid theory ($M_A^* = 2.76$). A subcritical shock is found to exhibit in our calculations a remarkably stationary behaviour after the usual transitory period. The shock is then purely resistive, and its width relates to the resistive length L_r. The only ion heating is adiabatic with $\gamma_i = 2$, and $V_{iy} = 0$ throughout the shock. The usual magnetosonic wavetrain [*Tidman and Krall*, 1971] is not observed, since no c/ω_{pe} scale is included in our calculation. The Rankine-Hugoniot relations are found to be well verified within an accuracy of 10%.

Very high Mach number regime ($M_A > 10$). The simulation leads to nonstationary structures above a certain threshold of M_A, $M_A^{**} \simeq 12$–13. For $M_A > M_A^{**}$, the shock front is found to move toward the right of the system with a velocity such that the effective Mach number in the shock rest frame falls a little below M_A^{**}. In addition, this value M_A^{**} is found to be rather insensitive to β_{i1}. This result may again be compared with the results of *Chodura* [1975] for unmagnetized ions. In that case no shock structure was obtained for $M_A > 10$, since above this value piston structure and shock structure were found to be indistinguishable. On the other hand, *Forslund and Freidberg* [1971] for the case of no resistivity and unmagnetized ions have derived an upper critical Mach number $M_A^{**} = 3.18$ above which all ions are reflected and no shock solution exists. The inclusion of resistivity, however, has the effect of increasing the critical Mach numbers M_A^* and M_A^{**}. It is well known in particular that for $\beta_{i1} = \beta_{e1} = 0$, M_A^* goes from 2. to 2.76 when resistivity is allowed [*Biskamp*, 1973]. However, the question of whether M_A^{**} is finite or infinite when resistivity is included has not yet been resolved. Although a possible inadequacy of the initial conditions cannot be excluded, our results together with Chodura's tend to suggest that M_A^{**} is actually finite and equal to 12–13 in the magnetized case for one-dimensional spatial variation. The existence of M_A^{**} is related to the inefficiency of dissipation mechanisms above a certain threshold. We have already noted that electron dissipation tends to saturate with M_A. This implies that the gyrating ions might be unable to provide the increase of ion kinetic pressure required to satisfy the Rankine-Hugoniot relations above a certain threshold of the Mach number.

5. SUMMARY AND DISCUSSION

In this section we summarize our main results and discuss them in relation to observational data of quasi-perpendicular bow shocks. Some remarks on laboratory experiments are also included. The empirical definition of quasi-perpendicular shocks refers to shocks for which the angle θ_{nB} between the upstream magnetic field and the shock normal exceeds 50° [*Dobrowolny and Formisano*, 1973]. Quasi-perpendicular shocks form a broad and rather homogeneous category, exhibit easily identifiable features, and resemble the perpendicular shock in being sharply defined [*Greenstadt and Fredricks*, 1979]. By using a version of our code which includes a small component of the magnetic field along the shock normal ($\theta_{nB} \simeq 80°$), we have obtained results that are very similar to those with θ_{nB} exactly equal to 90°. Thus the strictly perpendicular geometry investigated throughout this paper is actually not singular and may be used as a basis for a comparison with observational data of quasi-perpendicular shocks. It should be kept in mind, however, that whereas a rigorous comparison can be made with nearly perpendicular shocks ($80° \lesssim \theta_{nB} \lesssim 90°$), the comparison of the simulation results with more oblique shocks, still quasi-perpendicular, should be viewed with some skepticism, since a change of the physical processes in the shock can be expected as θ_{nB} decreases by a significant amount [*Biskamp*, 1973].

a. *The Reflected Gyrating Ion Stream; Ion Heating*

Preliminary observational results reported by *Paschmann et al.* [1981] for the November 7, 1977, shock crossing ($M_A \simeq 8$, $\beta_i \simeq 0.9$, $\beta_e \simeq 2.2$) indicate the presence of a gyrating stream of density about 20% of the upstream density in the foot region of the shock. This value is fairly consistent with our simulations, which give $\alpha \simeq 18\%$ for $M_A = 8$, $\beta_{e1} = \beta_{i1} = 1$ (see Figure 10). The maximum number of reflected ions in the simulations is about 32% (high M_A, low resistivity), in general agreement with laboratory experiments which have shown an upper limit of 35% for α or even less [*Chodura*, 1975].

The reflected stream observed by *Paschmann et al.* [1981] extends back into the downstream region and creates there a bimodal ion distribution. Such bimodal distributions in the bow shock were first observed by *Montgomery et al.* [1970] and confirmed by other experimenters [*Formisano and Hedgecock*, 1973; *Greenstadt et al.*, 1980]. The additional group of protons of the distribution is observed to have velocities approximately twice the upstream bulk speed near the shock front [*Montgomery et al.*, 1970], in good agreement with our results. Figure 1*e* shows, in fact, that the magnitude of the velocity of the gyrating stream is about 1.7 to 1.9 the upstream bulk speed. Although the high-energy peak of the bimodal distribution has been discussed in terms of a gyrating ion stream propagating across the magnetic field as early as 1971 [*Auer et al.*, 1971], this high-energy peak has been interpreted most commonly as a high-energy component along the field direction [*Greenstadt and Fredricks*, 1979]. Our results reproduce rather nicely the ion gyrating stream in the foot as well as in the downstream region (Figure 1*e*) and confirm the earlier interpretation of *Auer et al.* [1971]. The agreement is further reenforced when the ion distributions are displayed in the spacecraft reference frame (C. C. Goodrich, manuscript in preparation, 1982) and compared with the results of *Paschmann et al.* [1981].

Although the ion thermalization length is observed to be large compared with the ion gyroradius, the hybrid code is expected to underestimate the downstream ion thermalization rate. In particular, isotropization processes are missing in the code, since the ions do not undergo any heating in the field direction. Preliminary analytic results [*Papadopoulos,* 1981] indicate that instabilities driven by loss cone–like ion distributions due to the gyrating ions can produce thermalization in the direction perpendicular to the magnetic field, while the electromagnetic ion cyclotron instability [*Davidson and Ogden,* 1975] can produce energy transfer in the parallel direction and isotropization. These will be discussed in a forthcoming paper (C. S. Wu et al., manuscript in preparation, 1982).

b. *Time Dependence and Length Scales of the Overall Structure*

The use of multiple spacecraft in the ISEE experiment has permitted reliable length scale measurements of the bow shock thickness. It has been shown [*Russell and Greenstadt,* 1979] that moderately supercritical quasi-perpendicular bow shocks have reproducible features indicating structural stability over a time scale of a minute (typically $10^2\ \omega_{ci}^{-1}$). These features include a foot region, a principal sharp magnetic gradient, a postgradient overshoot, and a postovershoot relaxation (undershoot) in which the field falls below its downstream value. The simulation results are consistent with such a picture. After a transitory period lasting about a downstream ion gyroperiod, an overall structure of the shock is formed and persists in time; it includes the above listed features (foot, ramp, overshoot, undershoot; see, for example, Figure 2). Some oscillations do exist, particularly weak for a rather large upstream β_{i1} ($\beta_{i1} \simeq 1$) and quite significant for low β_{i1} ($\beta_{i1} \sim 0.1$), but at any rate they are not strong enough to destroy the overall structure; moreover, the shock front does not move significantly. In this sense our model does not support previous theoretical models of supercritical shocks in the magnetized case [*Biskamp and Welter,* 1972; *Morse,* 1976]. The quasi-stationary behavior observed in our simulations at large β_{i1} ($\beta_{i1} \simeq 1$) may also be related to the steady shock structures obtained in some high-β laboratory experiments [*Keilhacker et al.,* 1969, 1971]. Furthermore, we show (sec. 4*a*) that the sizes of the foot and the overshoot region are mainly determined by ion dynamics, whereas the thickness of the magnetic ramp is mainly determined by the resistivity (resistive length). What is usually referred to in the literature (i.e., for example, *Russell and Greenstadt* [1979]) as 'thickness of the shock' corresponds to the foot plus ramp in our model. The thicknesses of the foot and of the overshoot are observed to be of the order of c/ω_{pi} and 3 c/ω_{pi}, respectively [*Russell and Greenstadt,* 1979], whereas our calculations give 1.3–2.3 c/ω_{pi} for the foot and 4–7 c/ω_{pi} for the overshoot with M_A in the range 4–10 (Figure 9). These numbers are in reasonable agreement if we take into account the fact that the observed quasi-perpendicular shock crossing of *Russell and Greenstadt* [1979] has $\theta_{nB} \lesssim 70°$. The nearly perpendicular high Mach number ($M_A \sim 8$) shock crossing of November 7, 1977, agrees more closely with our results. From the UCLA magnetometer data and the known normal velocity of ISEE 1 with respect to the shock (7.5 km/s; J. D. Scudder, private communication, 1981), we infer a foot region thickness $\simeq 2.4$ c/ω_{pi} and an overshoot thickness $\simeq 6$ c/ω_{pi}, whereas our simulations give respectively $\sim$2.2 c/ω_{pi} and $\sim$5 c/ω_{pi} for $M_A = 8$ (Figure 9).

Another interesting observational feature is the presence in the overshoot of a large amplitude wave train of several cycles that scale as a fraction of c/ω_{pi} [*Russell and Greenstadt,* 1979]. It is likely that these fluctuations are simply the signature of the temporal variations that occur on the ion gyrotime scale in our simulations. A fictitious 'satellite' entering our simulated transition layer with a reasonable velocity (a few kilometers per second or, equivalently, $\sim 10^{-1}\ c/\omega_{pi}$ per ω_{pi}^{-1}) may be considered as motionless with respect to the shock structure on the ion gyrotime scale. The fluctuations recorded by this satellite are thus mainly temporal within the framework of our model. The level of the fluctuations are found to be in good agreement with the observations. The rms standard deviation of the magnetic field fluctuations for the shock crossing of November 5, 1977 ($M_A = 5.7$, $\beta_{i1} = 0.17$) is about 0.2 B_2 [*Greenstadt et al.,* 1980, Figure 1]. On the other hand, Figure 12 gives a rms value of 0.1 B_2 for $M_A = 6$, $\beta_{i1} = 0.1$ and $\eta/4\pi = 10^{-4}\ \omega_{pi}^{-1}$, a value which can be increased by typically a factor of 2 if the resistivity is reduced by a factor of 10^2–10^3.

c. *Electron Heating*

The hybrid code in its present form is not expected to lead to very accurate results as far as electron heating is concerned, both because of the simple model of resistivity assumed, and because important effects in the bow shock such as electron heat flux have been omitted in the fluid calculation of the electrons. In particular, we expect electron heating to be overestimated in our calculation, since the assumption of constant resistivity leads to further electron heating beyond the magnetic ramp; the effect is more pronounced at higher Mach numbers where the downstream region contains steep magnetic field gradients. In contrast, the observed enhanced fluctuations giving rise to anomalous resistivity typically have frequencies between the lower hybrid and the electron plasma frequency and occur primarily in the foot, ramp, and part of the overshoot region [*Greenstadt et al.,* 1980]. Furthermore, electron temperature measurements reveal [*Bame et al.,* 1979] that the profiles of T_e and n_e are often similar to one another and also similar to the profile of B, which indicates that no subsequent electron heating takes place after the magnetic field overshoot. This suggests that the resistivity should be 'turned off' beyond the overshoot region in our model. Nevertheless, the use of a phenomenological resistivity has led to the following conclusions.

1. The shock structure (foot, ramp, overshoot) is principally governed by ion dynamics and not by resistivity.
2. The amount of Ohmic dissipation in the ramp region is weakly dependent upon the magnitude of the resistivity, as are the number of reflected ions and the magnitude of the field overshoot. While the qualitative presence of resistivity is needed to provide energy dissipation, its actual form and magnitude appears to play a secondary role.
3. Two regimes for β_{e1} can be distinguished. When β_{e1} is less than 1, Ohmic heating prevails and the shock structure is essentially independent of β_{e1}. When β_{e1} is significantly larger than 1, compressional (adiabatic) heating prevails. The latter situation occurs most often in the bow shock, since β_{e1} does not change very much in the solar wind and is often greater than unity.

d. *Magnetic Deflection*

The foot region plays a crucial dynamic role in that reflected ions provide both an extra contribution to the electric potential barrier (potential overshoot) and a significant deceleration of the incoming ions by magnetic deflection (paper 1; also sections 3 and 4). The importance of magnetic deflection has been demonstrated experimentally with the observation of plasma rotation in a theta pinch by *Bengston et al.* [1977]. These authors have observed a large component of the average ion velocity in a direction orthogonal both to the field and to the shock normal, which is the signature of magnetic effects.

The presence of an isomagnetic jump, observed in laboratory experiments in the range $M_A \simeq 3$–5 and interpreted as an ion-acoustic subshock [*Eselevich et al.*, 1971; *Eselevich*, 1981], has not been observed in our simulations. This is not surprising, since the ion acoustic subshock scales as the electron Debye length, which is much shorter than the smallest scale we consider, the resistive length scale. This omission has probably no crucial consequences, since the isomagnetic jump is not expected to lead to significant ion heating [*Biskamp*, 1973].

e. Mach Number and β_i Dependence

The magnetic field and potential overshoots are intimately correlated to the reflected ions (paper 1). Figures 10 and 12 show that the magnetic field overshoot vanishes for $M_A < 3$. This corresponds roughly to the first critical Mach number beyond which ion reflection occurs. These figures show also that both the number of reflected ions and the field overshoot are increasing functions of M_A. The time average of the magnitude $(B_{max} - B_2)/B_2$ of the magnetic field overshoot increases from 0 at $M_A \simeq 3$ to about 0.5 for $M_A = 10$ (Figure 10) and can reach 1 for $M_A = 10$ and very small resistivities. This result is consistent with observations of planetary bow shocks [*Russell et al.*, 1981]. For a given M_A, the simulations show that the average in time of the magnetic field overshoot is independent of β_{e1} (section 4*b*) and rather independent of β_{i1} (compare Figure 10 and Figure 12). Since the field overshoot increases with M_A at constant $\beta_1 \equiv \beta_{e1} + \beta_{i1}$, this implies that for a given magnetosonic Mach number

$$M_S = M_A\left(1 + \frac{\gamma\beta_1}{2}\right)^{-1/2}$$

the field overshoot increases with β_1, which is also consistent with the results of *Russell et al.* [1981]. We note also that the fluctuations of the field overshoot about its time average become significant at low β_{i1} ($\beta_{i1} \sim 0.1$) and high M_A ($M_A \geq 8$).

The large-scale features of the post magnetic ramp region are determined primarily by the gyrating ions (paper 1). The results (Figure 9) show that the compression-rarefaction features of the downstream region scale as V_1/ω_{ci2}, i.e., the upstream bulk speed divided by the ion gyrofrequency computed with the downstream magnetic field. We find in particular that the thickness of the magnetic field overshoot scales as $\sim 3V_1/\omega_{ci2}$. Finally, we show that the kinetic energy per ion in the gyrating stream is about 3–3.5 times $m_iV_1^2/2$ in the near downstream region just beyond the magnetic ramp.

In the low Mach number, subcritical regime ($M_A \lesssim 3$), we have obtained essentially resistive shocks, characterized by a smooth and monotonic transition layer which scales with the resistive length. Ion reflection is absent, and the only ion heating is compressional (adiabatic). These results are in good agreement with fluid theory [*Tidman and Krall*, 1971] and with observations of quasi-perpendicular bow shocks or interplanetary shocks [*Greenstadt et al.*, 1975; *Formisano et al.*, 1973; *Greenstadt*, 1974; *Russell and Greenstadt*, 1979]. Such subcritical shocks are labeled 'laminar' when $\beta_1 \ll 1$ and quasi-turbulent when $\beta_1 \simeq 1$. It has been generally observed that, although the overall shock structure does not depend drastically on β_1 (ions + electrons), the $\beta_1 \simeq 1$ shocks exhibit more local irregularities in the magnetic field than low-β_1 shocks [*Formisano and Hedgecock*, 1973; *Russell et al.*, 1981]. On the other hand, we find in the simulations that moderately high ion β_{i1} (not the total β) give rise to more stable structures in the supercritical regime than low β_{i1}.

Very high beta structures have not been investigated in the present paper. We expect quite a different behavior when β_{i1} is such that a significant fraction of upstream particles have a negative velocity component along the shock normal, i.e., when β_{i1}/M_A^2 is larger than 1. Very high β shocks, although rare in the earth's bow shock, are observed to behave in a very irregular fashion [*Formisano et al.*, 1975].

Acknowledgments. We are grateful to A. Mangeney, C. Lacombe, and J. D. Scudder for very helpful discussions regarding unpublished ISEE data and to A. G. Sgro regarding hybrid codes. This work was supported by NASA solar terrestrial theory grant NAGW-81.

The editor thanks G. Paschmann and D. W. Forslund for their assistance in evaluating this paper.

REFERENCES

Auer, P. L., and W. H. Evers, Collision-free shock formation in finite temperature plasmas, *Phys. Fluids, 14,* 1177, 1971.

Auer, P. L., H. Hurwitz, Jr., and R. W. Kilb, Large amplitude magnetic compression of a collision-free plasma, 2, Development of a thermalized plasma, *Phys. Fluids, 5,* 298, 1962.

Auer, P. L., R. W. Kilb, and W. F. Crevier, Thermalization of the earth's bow shock, *J. Geophys. Res., 76,* 2927, 1971.

Bame, S. J., J. R. Asbridge, J. T. Gosling, M. Halbig, G. Paschmann, N. Sckopke, and H. Rosenbauer, High temporal resolution observations of electron heating at the bow shock, *Space Sci. Rev., 23,* 75, 1979.

Bengston, R. D., S. A. Eckstrand, A. G. Sgro, and C. W. Nielson, Plasma rotation during implosion in a θ pinch, *Phys. Rev. Lett., 39,* 884, 1977.

Biskamp, D., Collisionless shock waves in plasmas, *Nucl. Fusion, 13,* 719, 1973.

Biskamp, D., and H. Welter, Numerical studies of magnetosonic collisionless shock waves, *Nucl. Fusion, 12,* 663, 1972.

Chodura, R., A hybrid fluid-particle model of ion heating in high Mach-number shock waves, *Nucl. Fusion, 15,* 55, 1975.

Davidson, R. C., and N. A. Krall, Anomalous transport in high temperature plasma with application to solenoidal fusion systems, *Nucl. Fusion, 17,* 1313, 1977.

Davidson, R. C., and J. M. Ogden, Electromagnetic ion cyclotron instability driven by an energy anisotropy in high beta plasmas, *Phys. Fluids, 18,* 1045, 1975.

Dobrowolny, M., and V. Formisano, The structure of the earth's bow shock, *Rev. Nuovo Cim, 3,* 419, 1973.

Eselevich, V. G., Bow shock structure from laboratory and satellite experimental results, *Preprint 19-81,* Siberian Inst. of Terr. Magn., Ionos. and Radio Wave Propag., Irkutsk, USSR, 1981.

Eselevich, V. G., A. G. Es'kov, R. K. Kurtmullaev, and A. I. Malyutin, Isomagnetic discontinuity in a collisionless shock wave, *Sov. Phys. JETP, 33,* 1120, 1971.

Formisano, V., The physics of the earth's collisionless shock wave, *J. Phys., 38,* C6-65, 1977.

Formisano, V., and P. C. Hedgecock, On the structure of the turbulent bow shock, *J. Geophys. Res., 78,* 6522, 1973.

Formisano, V., G. Moreno, F. Palmiotto, and P. C. Hedgecock, Solar wind interaction with the earth's magnetic field, *J. Geophys. Res., 78,* 3714, 1973.

Formisano, V., C. T. Russell, J. D. Means, E. W. Greenstadt, F. L. Scarf, and M. Neugebauer, Collisionless shock waves in space: A very high-beta structure, *J. Geophys. Res.*, *80*, 2030, 1975.

Forslund, D., and J. P. Freidberg, Theory of laminar collisionless shocks, *Phys. Rev. Lett.*, *27*, 1189, 1971.

Greenstadt, E. W., Structure of the terrestrial bow shock, in *Solar Wind Three*, edited by C. T. Russell, p. 440, Institute of Geophysics and Planetary Physics, University of California, Los Angeles, 1974.

Greenstadt, E. W., and R. W. Fredricks, Shock systems in collisionless space plasmas, in *Solar System Plasma Physics*, vol. III, edited by L. J. Lanzerotti, C. F. Kennel, and E. N. Parker, p. 3, North-Holland, Amsterdam, 1979.

Greenstadt, E. W., C. T. Russell, F. L. Scarf, V. Formisano, and M. Neugebauer, Structure of the quasi-perpendicular, laminar bow shock, *J. Geophys. Res.*, *80*, 502, 1975.

Greenstadt, E. W., C. T. Russell, J. T. Gosling, S. J. Bame, G. Paschmann, G. K. Parks, K. A. Anderson, F. L. Scarf, R. R. Anderson, D. A. Gurnett, R. P. Lin, C. S. Lin, and H. Reme, A macroscopic profile of the typical quasi-perpendicular bow shock: ISEE 1 and 2, *J. Geophys. Res.*, *85*, 2124, 1980.

Hamasaki, S., N. A. Krall, C. E. Wagner, and R. N. Byrne, Effect of turbulence on theta pinch modeling by hybrid numerical models, *Phys. Fluids*, *20*, 65, 1977.

Keilhacker, M., M. Kornherr, and K. H. Steuer, Observation of collisionless plasma heating by strong shock waves, *Z. Phys.*, *223*, 385, 1969.

Keilhacker, M., M. Kornherr, H. Niedermeyer, K. H. Steuer, and R. Chodura, Plasma physics and controlled nuclear fusion research, *IAEA Bull.*, *3*, 265, 1971.

Leroy, M. M., C. C. Goodrich, D. Winske, C. S. Wu, and K. Papadopoulos, Simulations of a perpendicular bow shock, *Geophys. Res. Lett.*, *8*, 1269, 1981.

Mason, R. J., Ion and electron pressure effects on magnetosonic shock formation, *Phys. Fluids*, *15*, 1082, 1972.

Montgomery, M. D., J. R. Asbridge, and S. J. Bame, VELA 4 plasma observations near the earth's bow shock, *J. Geophys. Res.*, *75*, 1217, 1970.

Morse, D. L., A model for ion thermalization in the earth's bow shock, *J. Geophys. Res.*, *81*, 6126, 1976.

Papadopoulos, K., Comments on high Mach number perpendicular shock, in *Proceedings of the 1981 Varenna School of Plasma Astrophysics*, p. 409, North-Holland, Varenna, Italy, 1981.

Papadopoulos, K., C. E. Wagner, and I. Haber, High-Mach-number turbulent magnetosonic shocks, *Phys. Rev. Lett.*, *27*, 982, 1971.

Paschmann, G., N. Sckopke, G. Haerendel, S. J. Bame, J. R. Asbridge, and J. T. Gosling, Structure of ion distributions across the earth's bow shock (abstract), *Eos Trans. AGU*, *62*, 363, 1981.

Paul, J. W. M., G. C. Goldenbaum, A. Ioyoshi, L. S. Holmes, and R. A. Hardcastle, Measurements of electron temperatures produced by collisionless shock waves in magnetized plasma, *Nature*, *216*, 363, 1967.

Phillips, P. E., and A. E. Robson, Reflection of ions from perpendicular shocks, *Phys. Rev. Lett.*, *29*, 154, 1972.

Russell, C. T., and E. W. Greenstadt, Initial ISEE magnetometer results: Shock observations, *Space Sci. Rev.*, *23*, 3, 1979.

Russell, C. T., M. M. Hoppe, and W. A. Livesey, Overshoots in planetary bowshocks, *Inst. Publ. 2182*, Inst. of Geophys. and Planet. Phys., Univ. of Calif., Los Angeles, 1981.

Sgro, A. G., and C. W. Nielson, Hybrid model studies of ion dynamics and magnetic field diffusion during pinch implosions, *Phys. Fluids*, *19*, 126, 1976.

Sherwell, D., and R. A. Cairns, Ion dynamics in a perpendicular collisionless shock, *J. Plasma Phys.*, *17*, 265, 1977.

Tidman, D. A., and N. Krall, *Shock Waves in Collisionless Plasmas*, John Wiley-Interscience, New York, 1971.

Wu, C. S., Physical mechanisms for turbulent dissipation in collisionless shock waves, *Space Sci. Rev.*, in press, 1982.

(Received February 4, 1982;
revised April 26, 1982;
accepted April 27, 1982.)